Journal of Materials Chemistry C

ROYAL SOCIETY OF CHEMISTRY

COMMUNICATION

View Article Online
View Journal | View Issue

Cite this: J. Mater. Chem. C, 2022, 10, 12191

Received 14th June 2022,
Accepted 9th August 2022

DOI: 10.1039/d2tc02498e

rsc.li/materials-c

Ultrasensitive turn-on luminescence humidity sensor based on a perovskite/zeolite composite†

Yu-Jie Gao,[a] Giacomo Romolini,[b] Haowei Huang,[a] Handong Jin,[b] Rafikul Ali Saha,[a] Biplab Ghosh,[a] Michiel De Ras,[b] Chunhua Wang,[b] Julian A. Steele,[ac] Elke Debroye,[b] Johan Hofkens[b] and Maarten B. J. Roeffaers*[a]

Recently, the detection and quantification of humidity has attracted great interest, but for fluorescence sensing of humidity, it is still a challenge to achieve high-performance. Here, we report an ultrasensitive and high-performing luminescence humidity sensor based on perovskite/zeolite composite, Cs_4PbBr_6/FAU-Y. The zeolite FAU-Y acts as a support for dispersing amorphous Cs_4PbBr_6 nanoparticles (11 ± 2 nm), which rapidly undergo a moisture-mediated transformation into a highly luminescent $CsPbBr_3$ perovskite, due to the hydrophilic nature of the zeolite substrate. The composite exhibits strong fluorescence response ($(I-I_0)/I_0$) (992 for 98% RH, 91.7 for 7% RH), good linearity, low detection limit (0.56% RH), while producing highly reproducible and stable optical signals. Test paper embedded with the moisture sensitive composite yields a simple and reliable naked-eye method for detecting moisture exposure within anhydrous products and dry storage environments. This work showcases a unique concept to develop turn-on humidity sensors based on the bright metal halide perovskite luminescence, thus promoting innovative practical applications outside their typical scope of applications such as solar cells, photodetectors, or light emitting diodes (LEDs).

Humidity sensing plays an important role in monitoring moisture exposure during anhydrous processes and product storage.[1,2] Traditional methods for the determination of humidity are based on changes in the electrical properties of various materials such as ceramics, organic polymers, and semiconductive metal oxides.[3] However, these methods rely on electronics for moisture detection. Changes in optical properties have been considered a reliable and simple alternative owing to their high sensitivity and intuitive visual response.[4,5] Thus, recent research has focussed on developing fluorescent and colorimetric sensors.[2,3] Compared to colorimetric sensors, fluorescent sensors are generally more sensitive.[3] Within the class of fluorescent sensors, turn-on sensors can reach higher responses and are more reliable than turn-off sensors, which are limited by the maximum quenching value (≤ 1) and competition of photobleaching.[4,5] Until now, many optical humidity sensors have been reported such as organic fluorescent molecules, graphene composites, photonic crystals, zeolites, and metal–organic frameworks.[3,6] Nevertheless, current optical humidity sensing materials have several disadvantages including high cost, weak luminescence, slow responsivity, and low sensitivity.[2,3,6,7]

Metal halide perovskites (MHPs) are highly promising semiconductors that adopt a general formula of ABX_3 ($A = CH_3NH_3^+$, Cs^+, or $CH(NH)_2^+$; $B = Pb^{2+}$, Sn^{2+}; $X = Cl^-$, Br^-, I^-). MHPs have already been applied to various optoelectronic devices due to their outstanding optoelectronic characteristics.[8–11] MHPs have also been employed for humidity sensing but mostly based on changes in electronic properties.[12–21] Until now, luminescence moisture sensors based on MHPs are still in infancy.[14] For example, organic–inorganic MHP-based fluorescent humidity sensors not only show poor performance at low relative humidity (RH), but also degrade in moisture-rich environments.[14,22] Even the luminescence turn-off sensor based on highly emissive $CH_3NH_3PbBr_3$ shows poor humidity sensitivity and, due to the instability under moisture conditions, the sensor is not reliable for longer periods.[22] Recently $CsPbBr_3$ loaded in zeolite EMT (EMT-$CsPbBr_3$) was reported for humidity detection, however, the reported response and sensitivity are still low.[23]

Over the past few years, all-inorganic $CsPbX_3$ (X = Cl, Br, I) have drawn much attention because of their high chemical and thermal stability.[8,24] Interestingly, a related class of non-luminescent materials, Cs_4PbX_6 share structural similarity *e.g.*, the presence of $[PbX_6]^{4-}$ octahedral unit, and can be converted into $CsPbX_3$ and CsX in the presence of polar molecules such as

[a] Department of Microbial and Molecular Systems, Centre for Membrane Separations, Adsorption, Catalysis and Spectroscopy for Sustainable Solutions (cMACS), KU Leuven, Celestijnenlaan 200F, 3001 Leuven, Belgium. E-mail: maarten.roeffaers@kuleuven.be
[b] Department of Chemistry, Faculty of Sciences, KU Leuven, Celestijnenlaan 200F, 3001 Leuven, Belgium
[c] School of Mathematics and Physics, The University of Queensland, Brisbane, QLD, 4072, Australia

† Electronic supplementary information (ESI) available: Experimental section (materials, measurements, and syntheses), and additional tables (Tables S1 and S2) and graphics (Fig. S1–S16). See DOI: https://doi.org/10.1039/d2tc02498e

water.[25–29] Taking into consideration that non-luminescent Cs_4PbBr_6 could transform to stable and bright green-emitting $CsPbBr_3$ when exposed to water, Cs_4PbBr_6 could be an ideal candidate for developing turn-on fluorescent humidity sensors based on MHPs. To design an ultrasensitive humidity sensor, our strategy is to increase the contact between water and the water-sensitive Cs_4PbBr_6 by depositing small nanocrystals on a hygroscopic substrate material. Within this scenario, zeolite FAU-Y is ideal for promoting Cs_4PbBr_6 to $CsPbBr_3$ transformation because it is strongly hydrophilic and has a relatively large water adsorption capacity within its porous network, even at low partial pressures. In this work, we synthesized Cs_4PbBr_6/FAU-Y, with amorphous Cs_4PbBr_6 nanoparticles (NPs) well-dispersed on the surface of hydrophilic zeolite FAU-Y, and then investigate the fluorescence enhancement induced by humidity. The fluorescence intensity rapidly increased when Cs_4PbBr_6/FAU-Y was exposed to humidity in a wide range of 7% to 98% RH. Our material achieved the highest fluorescence response value to date, which is at least 50-fold higher than other MHP based fluorescent humidity sensors (Table S2, ESI†).[22,23,30] The sensitivity of our sensor is 11.8/RH% at high levels of RH (17–98%) and 12.6/RH% for low RH (<17%), while achieving very low limit of detection (0.56% RH). Furthermore, a fluorescent turn-on test paper of this composite material provides a simple and reliable naked-eye humidity detection method even for low RH 7%.

To generate well-dispersed Cs_4PbBr_6 nanoparticles on the FAU-Y surface, we developed an *in situ* growth method (Fig. 1a). First, FAU-Y zeolite was exchanged with a concentrated aqueous CsBr solution. In this step, Na^+ of FAU-Y was partly exchanged by Cs^+ to produce Cs^+/Na^+-FAU-Y with a molar ratio of Cs^+/Na^+ = 4.93; as determined by atomic absorption spectroscopy (AAS) (Table S1, ESI†). Actually, part of Cs^+ was found adsorbed on the FAU-Y surface. Indeed, an excess amount of CsBr was used for the exchange in order to yield a stoichiometric amount for the subsequent synthesis of Cs_4PbBr_6. Thus, considering the amount of adsorbed Cs^+, we calculated the Cs^+/Na^+ exchange efficiency to be 67.9% (details on the calculations can be found in ESI†). Then, the dry Cs^+/Na^+-FAU-Y was introduced into a $PbBr_2$ solution, with a stoichiometric ratio of Cs^+ to Pb^{2+} is 5.60 : 1. During this step, some Cs^+ is released from Cs^+/Na^+-FAU-Y. These Cs^+ ions are necessary for the *in situ* formation of well-dispersed Cs_4PbBr_6 nanoparticles anchored on zeolite FAU-Y. The details of the synthesis method are provided in ESI† and Fig. S1. Care needs to be taken to perform the synthesis in complete absence of water. The obtained Cs_4PbBr_6/FAU-Y white composite, which is non-luminescent, converts rapidly to a bright yellow material under ambient conditions and displays a strong green luminescence under 366 nm UV illumination (Fig. 1b and c).

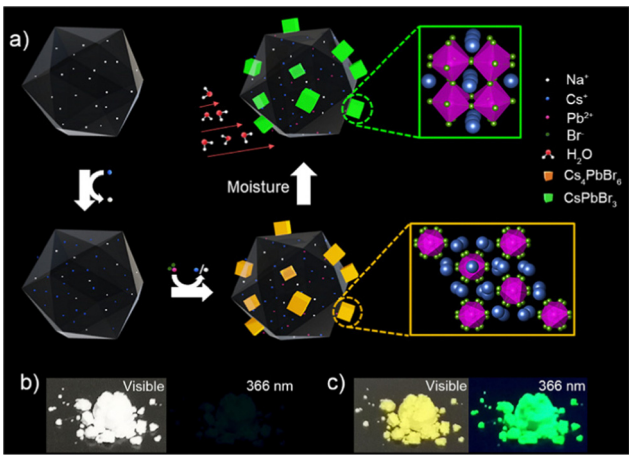

Fig. 1 Development of a metal halide perovskite-based turn-on humidity sensor starting from a non-luminescent precursor Cs_4PbBr_6. (a) Schematic illustration of the *in situ* growth method of Cs_4PbBr_6/FAU-Y composite and the conversion of non-luminescent Cs_4PbBr_6 into the green-fluorescent $CsPbBr_3$ in the presence of moisture. The *in situ* growth of Cs_4PbBr_6 involves the introduction of Cs^+ in the FAU-Y *via* ion-exchange followed by the addition of $PbBr_2$ leading to Cs_4PbBr_6 formation (details see Fig. S1 and Experimental section, ESI†). The transformation of Cs_4PbBr_6 to the $CsPbBr_3$ occurs in presence of moisture and the process is enhanced by the presence of FAU-Y. Photographs of the synthesized Cs_4PbBr_6/FAU-Y composite powder under visible light and UV light at 366 nm before (b) and after (c) exposure to air.

Detailed structural and compositional characterizations were carried out at different stages of Cs_4PbBr_6/FAU-Y composite formation to understand the underlying processes. The positions of the Bragg peaks (*hkl* planes) are identified using the Le Bail method which are depicted in Fig. 2a. The XRD data of the pristine FAU-Y and Cs^+/Na^+-FAU-Y can be fitted using same space group $Fd\bar{3}m$ which clearly indicate the incorporation of Cs^+ in the position of Na^+. Compared to the pristine FAU-Y, we identify some modification in the intensity of the diffraction peaks of the Cs^+/Na^+-FAU-Y XRD data. Moreover, all the Bragg peaks of Cs_4PbBr_6/FAU-Y before exposure to air are also described by a single $Fd\bar{3}m$ space group, signifying the amorphous nature of Cs_4PbBr_6. The UV-Vis absorption spectrum of the pristine Cs_4PbBr_6/FAU-Y in dry toluene solution, on the other hand, shows a sharp absorption peak at 314 nm, indicating the presence of Cs_4PbBr_6 in the composite (Fig. 2b).[25,31] The Cs : Pb molar ratio as calculated by AAS was found to be 6.50 : 1, which is in agreement with its CsBr-rich nature (Table S1, ESI†). Transmission electron microscopy (TEM) and high-resolution transmission electron microscopy (HRTEM) further support the amorphous nature of the Cs_4PbBr_6 NPs. As shown in Fig. 3a, b, and Fig. S4, (ESI†), Cs_4PbBr_6 NPs with an average size of 11 ± 2 nm, are formed on the surface of the zeolite. Closer inspections of the Cs_4PbBr_6 NPs were carried out using HRTEM that show the absence of diffraction peaks in the electron diffraction (Fig. 3c (inset)). The measurement indicates the amorphous nature of Cs_4PbBr_6 NPs which is quite different from previously reported crystalline Cs_4PbBr_6 NPs.[25]

After exposure to moist air, a bright yellow material is formed and the XRD pattern of the composite contains the characteristic peaks of both the Cs^+/Na^+-FAU-Y and the orthorhombic phase of $CsPbBr_3$ (Fig. 2a). No reflections from CsBr were found in the XRD pattern, suggesting no crystalline CsBr product was formed during moisture exposure.[26] The UV-Vis

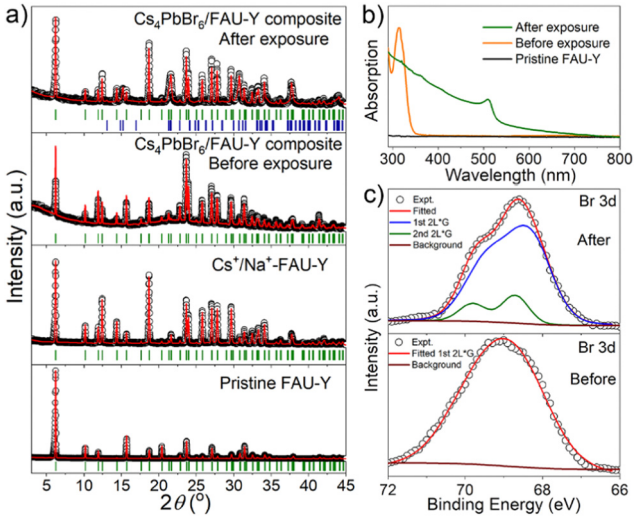

Fig. 2 (a) Le-Bail fitted XRD patterns of pristine FAU-Y, Cs^+/Na^+-FAU-Y, Cs_4PbBr_6/FAU-Y composite before and after exposure to air. Open black circles represent the experimental data, and the continuous red lines represent the calculated pattern. Vertical green and blue lines indicate the Bragg positions for all the samples. For Cs_4PbBr_6/FAU-Y composite after exposure to air, green Bragg peaks are attributed to the Cs^+/Na^+-FAU-Y phase and the blue Bragg peaks are appearing due to the orthorhombic phase of $CsPbBr_3$. (b) Absorption spectra of Cs_4PbBr_6/FAU-Y before and after exposure to air and pristine FAU-Y in the toluene solution. (c) Br 3d core level XPS spectra (black open circles) along with the fitting (red solid lines) of Cs_4PbBr_6/FAUY before and after exposure to air for 2 h. Brown lines represent the Shirley background. The blue line signifies one spin–orbit doublet and the green one indicates another spin–orbit doublet.

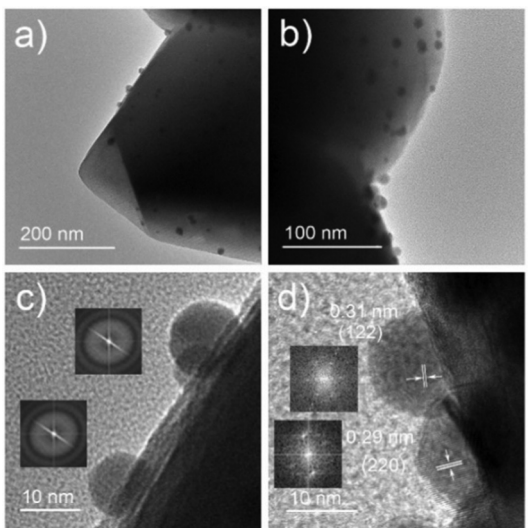

Fig. 3 (a and b) TEM images of Cs_4PbBr_6/FAU-Y composite. (c and d) HRTEM images of Cs_4PbBr_6/FAU-Y composite before and after short exposure to air. The black dots are perovskite particles. The insets of (c and d) are the electron diffraction diagrams of perovskite particles, respectively.

absorption spectrum of Cs_4PbBr_6/FAU-Y after exposure to air also shows the characteristic absorption peak of $CsPbBr_3$ (Fig. 2b).[25,31] Several clear diffraction spots are visible in HRTEM image that can be attributed to orthorhombic $CsPbBr_3$ in line with the bulk powder XRD experiments (Fig. 3d). The HRTEM also reveals the characteristic lattice spacing of about 0.29 nm and 0.31 nm, which corresponds to the *d*-spacing of (200) and (122) lattice planes of orthorhombic $CsPbBr_3$, respectively. This observation was confirmed by performing HRTEM of Cs_4PbBr_6/FAU-Y that was wetted with a trace of water (Fig. S5, ESI†). Furthermore, X-ray photoelectron spectroscopy (XPS) was also carried out before and after exposure to air to understand the bonding environment (Fig. 2c and Fig. S6, S7, ESI†). As shown in Fig. 2c, prior to air exposure, the Br 3d peak of Cs_4PbBr_6/FAU-Y composite has been fitted by a single spin–orbit doublet (two convolutions of a Lorentzian and a Gaussian peak: 2L*G) (gap between $d_{5/2}$ and $d_{3/2}$ ~ 1.07 eV; and ratio of $d_{5/2}$ and $d_{3/2}$ ~1.5), while after exposure, it has been fitted using two spin–orbit doublet (blue and green), indicating two different environments of Br ions. The blue doublet peak can be related to the Br^- in $CsPbBr_3$, while the green doublet peak most likely belong to the Br^- of CsBr.[32] All the results indicate an *in situ* growth of amorphous Cs_4PbBr_6 on the FAU-Y surface, which is quite different from the recent report where $CsPbBr_3$ nanocrystals are formed inside the pores of zeolite EMT.[23] Before exposure to moisture, Cs_4PbBr_6/FAU-Y in hexane solution has almost no visible emission like pure Cs_4PbBr_6 NPs (Fig. S8, ESI†). Indeed, it is only after exposure to humidity that the MHP precursor transforms to form the crystalline and highly luminescent $CsPbBr_3$ and CsBr. Therefore, the transformation process can be summarized as follows:

$$Cs_4PbBr_6 \xrightarrow{H_2O_{(g)}} CsPbBr_3 + 3CsBr$$

The Cs_4PbBr_6 can be regarded as a CsBr-rich structure with high ion-diffusion property.[25] Owing to the high solubility of CsBr in water and the hygroscopicity of FAU-Y, the Cs_4PbBr_6 could easily convert to $CsPbBr_3$ under ambient conditions. This moisture-triggered conversion results in a largely improved humidity sensitivity compared to other MHP-based humidity sensors.[22,23]

The humidity sensing ability of Cs_4PbBr_6/FAU-Y composite was studied systematically. The response (R) is a significant parameter for a sensor, which is defined as $R = (I-I_0)/I_0$,[33,34] where I is the photoluminescence (PL) intensity of the sensor at different RH conditions, while I_0 is the value of the dry sensor. The sensitivity (S) is defined as $S = \Delta R/\Delta RH$, which is the slope of the calibration curve.[21,35]

Fast response to humidity changes is a key aspect for detecting moisture leaks. Here, we evaluated the time dependent response of Cs_4PbBr_6/FAU-Y upon exposure to different RH. The response values were calculated at 523 nm PL emission. The pristine Cs_4PbBr_6/FAU-Y is almost non-luminescent but shows an ultralow emission peak at around 523 nm, which might be due to trace $CsPbBr_3$ formed during synthesis process (inset of Fig. S12c, ESI†). As shown in Fig. 4a, the response increases rapidly and reaches to the maximum value of 992

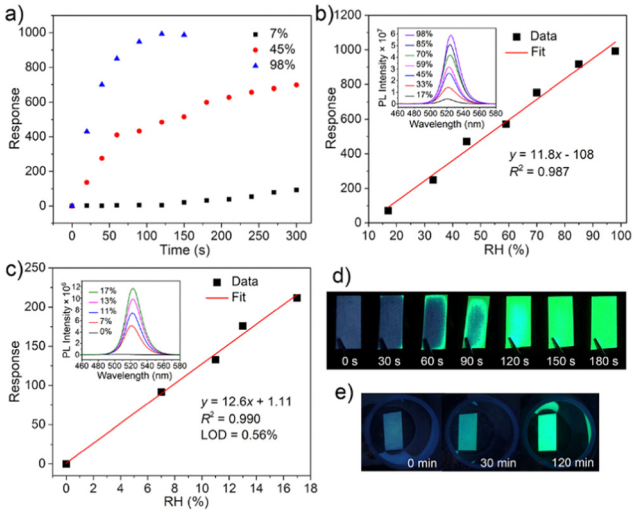

Fig. 4 (a) Response changes of Cs_4PbBr_6/FAU-Y composite upon exposure to different RH conditions. Linear curve between the response and RH of Cs_4PbBr_6/FAU-Y composite after 120 s exposure (b) and 300 s exposure (c). The insets of (b) and (c) show humidity dependent emission spectra of Cs_4PbBr_6/FAU-Y composite after exposure at different RHs for 120 s and 300 s, respectively. (d) Photographs of Cs_4PbBr_6/FAU-Y-based test papers for visible fluorescent detection of humidity. Unused test paper and test paper after exposure to air (35% RH) for 30 s, 60 s, 90 s, 120 s, 150 s, and 180 s under 366 nm UV light. (e) Unused test paper and test paper after exposure to 7% RH moisture condition for 30 min and 120 min under 366 nm UV light.

after 120 s at RH of 98%. When the RH is 45%, the response is fast for the first minute, after which it increases slowly. This is due to the gradual conversion of the Cs_4PbBr_6 precursor, which is also supported by the time-dependent reflectance results (Fig. S9, ESI†). When the RH decreases to 7%, the response is slower but still reaches a high value of 91.7 after 300 s.

The humidity dependent photoluminescence of the Cs_4PbBr_6/FAU-Y composite was also investigated. As shown in Fig. 4b, the responsivity of the composite is linear (S = 11.8/RH%, R^2 = 0.987) in the RH range 17% to 98% (exposure time of 120 s) (Fig. 4c). The increasing PL intensity is accompanied by a slight red-shift in the emission maximum from 521 nm to 525 nm which is related to the increasing size of the green-emitting $CsPbBr_3$ NPs with higher RH. For lower humidity range (<17%), the response was measured after an exposure time of 300 s. The corresponding response curve (Fig. 4c) reflects a highly linear relationship between fluorescence response and RHs with a sensitivity of 12.6/RH% and R^2 = 0.990. The limit of detection (LOD) of the sensor is calculated to be as low as 0.56% RH according to the $3\sigma/S$, where σ is the standard deviation of the blank signal (n = 20), and S is the slope of the linearity (sensitivity). Overall, our sensor possesses high humidity responses and sensitivities at both high (992 for 98% RH, 11.8/RH%) and low RH (91.7 for 7% RH, 12.6/RH%) range, which is at least 50-fold response and 60-fold sensitivity superior than other MHP based fluorescent humidity sensors ($CH_3NH_3PbBr_3$ and EMT-$CsPbBr_3$) (Table S2, ESI†).[22,23,30] Compared to other humidity sensors, Cs_4PbBr_6/FAU-Y fluorescence turn-on sensor shows much higher sensitivity or a lower LOD (Table S2, ESI†).[7,16–23,30,36–40] Furthermore, the converted $CsPbBr_3$ shows good moisture stability at both low and high RH testing conditions. It maintains a bright luminescence even after storing for 1 week at 45% RH (Fig. S10, ESI†). However, XRD pattern shows additional peaks originating from the $CsPb_2Br_5$ (Fig. S11, ESI†) which is a partial dissolution product of $CsPbBr_3$. This partial dissolution at the surface and the formation of a $CsPb_2Br_5$ shell layer has been reported to protect the green-emitting $CsPbBr_3$ which might explain the excellent fluorescence stability of our sensor.[29,41,42] Although the humidity sensor showed good stability in high RH conditions, the water-induced decomposition of MHPs still occurs after immersion in liquid water.

To examine the reproducibility of the Cs_4PbBr_6/FAU-Y sensor, the relationship between fluorescence response and RH of different synthesis batches was examined. Compared to the above calibration curve, the humidity dependence equations based on the product of different batches show similar values of S (11.9/RH% for high RH range, 12.4/RH% for low RH range) and LOD (0.57% RH) (Fig. S12, ESI†). The results confirm that our humidity sensor possesses good repeatability and reliability.

To investigate the importance of the Cs_4PbBr_6 nanoparticle size and the use of a hygroscopic support, FAU-Y, the response of Cs_4PbBr_6/FAU-Y was compared to pure Cs_4PbBr_6 NPs, Cs_4PbBr_6 large particles (LPs), and Cs_4PbBr_6/SiO_2; the detailed characterization of these materials can be found in ESI† (Fig. S13–S16). As shown in Fig. 5, the fluorescence intensity of Cs_4PbBr_6 NPs (23 ± 2 nm) has a very slow, but measurable response after exposure to 45% RH for 20 h which is orders of magnitude slower than when deposited on the zeolite support. The Cs_4PbBr_6 LPs (700 ± 300 nm) even show almost no fluorescence response after such a long exposure. Clearly, small Cs_4PbBr_6 NPs are essential to improve the transformation dynamics into $CsPbBr_3$. To further clarify the role of the hygroscopic support, Cs_4PbBr_6/FAU-Y was compared to Cs_4PbBr_6/SiO_2. While the fluorescence response for the former rapidly increases after humidity exposure and possesses a high response: R = 1038 after 30 min, Cs_4PbBr_6 NPs on the nonporous SiO_2 shows much slower response: R = 14 after 60 min. Particularly notable is the excellent response value of 1038 of Cs_4PbBr_6/FAU-Y composite, representing

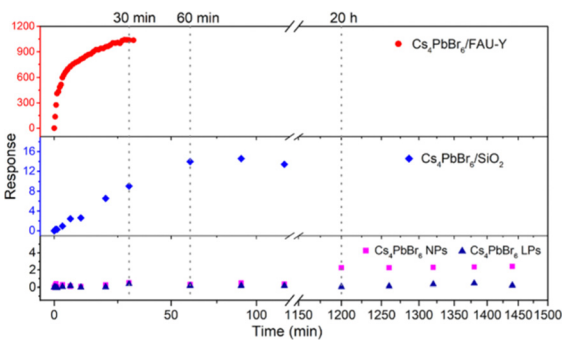

Fig. 5 Response changes of Cs_4PbBr_6/FAU-Y, Cs_4PbBr_6/SiO_2, Cs_4PbBr_6 NPs, and Cs_4PbBr_6 LPs upon exposure to 45% RH condition.

56-fold improvement over the highest response value for humidity fluorescent sensing to date (~18 of EMT-$CsPbBr_3$) (Table S2, ESI†).[2,3,6,22,23,30] Hence, the excellent sensing performance of Cs_4PbBr_6/FAU-Y can be attributed to the synergistic effect of (1) the nanosized Cs_4PbBr_6 that promote rapid transformation to bright green-emissive $CsPbBr_3$, and (2) the hygroscopic 3D porous support material that enhance the conversion speed.

In view of the merits of our composite material, it holds great promise for practical applications such as detecting moisture leaks. A fluorescence test paper was prepared by impregnating a Whatman filter paper with a size of about 1×2 cm^2 in 80 mg of Cs_4PbBr_6/FAU-Y suspended in 1 mL of extra dry hexane suspension and subsequent drying it. When the test paper was exposed to 35% RH, a green fluorescence can be easily observed within 30 s by naked eye under 366 nm UV light irradiation and the test paper became completely luminescent in 2 minutes (Fig. 4d). The test process can be appreciated from the video provided in the ESI† (Video S1). In addition, the test paper was also used in dry conditions (7% RH) where a visual response appears after 30 min (Fig. 4e). Compared to the turn-off $CH_3NH_3PbBr_3$ based sensing film, which shows no change at RH of 7% for 1 h, our fluorescence test paper is an outstanding probe for moisture leaks of anhydrous and ultra-dry condition.[22] It is worth noting that the change in color of our test paper, from white to yellow, can also be observed by the naked eye under visible light. The test paper is single-use, allowing to keep the signal of a possible moisture leakage accident and could provide higher protection to water-sensitive materials. All the results highlight the performance of low-cost Cs_4PbBr_6/FAU-Y test paper as a moisture leak sensor.

Conclusions

In summary, we introduced hygroscopic FAU-Y to promote the transformation from Cs_4PbBr_6 to $CsPbBr_3$ to make a sensitive humidity sensor. Our strategy prevents the water-induced fluorescence quenching of perovskites. In contrast, a fluorescence enhancement sensor with good luminescence stability was developed. Moreover, our composite humidity sensor, consisting of the MHP precursor, shows at least 50-fold improved response and 60-fold higher sensitivity than previous works that used water-induced property changes of the MHP. The advantages of Cs_4PbBr_6/FAU-Y include (i) low cost, (ii) ultrahigh responsivity (the highest fluorescence response value of 1038 to date), (iii) wide linear range (7–98% RH), (iv) high sensitivity (11.8/RH% for high RH and 12.6/RH% for low RH), (v) low limit of detection (0.56% RH), (vi) good reproducibility and moisture stability. This work provides a unique idea to develop MHPs luminescent humidity sensors, which can also prompt researchers to pay attention to the fluorescence sensing properties of MHPs.

Author contributions

Y. G. performed the material synthesis and characterization, analysed the data, and prepared the original draft; G. R., H. J., H. H. performed the XRD, the SEM-EDX and TEM measurements respectively; G. R., M. D. R. and C. W. supported with the material synthesis; J. A. S. and R. A. S. analysed the XRD and XPS data; J. A. S. helped with the critical assessment of the data; J. A. S., E. D., and J. H. supervised the project; B. G. and M. R. supervised the project and reviewed and edited the draft. All authors contributed to discussion of results and commented on the manuscript.

Conflicts of interest

There are no conflicts to declare.

Acknowledgements

This work was financially supported by the Research Foundation – Flanders (FWO grant no. G098319N, 11C6922N, 12Y7221N and V400622N), the KU Leuven Research Fund (C14/19/079, iBOF-21-085 PERSIST, and STG/21/010), KU Leuven Industrial Research Fund (C3/19/046) and the Flemish government through long term structural funding Methusalem (Meth/15/04). Yu-Jie Gao sincerely acknowledges the China Scholarship Council (CSC) for a doctoral fellowship (Grant number 201806650002).

Notes and references

1 H. Farahani, R. Wagiran and M. N. Hamidon, *Sensors*, 2014, **14**, 7881–7939.
2 S. Mishra and A. K. Singh, *Coord. Chem. Rev.*, 2021, **445**, 214063.
3 H. S. Jung, P. Verwilst, W. Y. Kim and J. S. Kim, *Chem. Soc. Rev.*, 2016, **45**, 1242–1256.
4 Z.-F. Wu, B. Tan, E. Velasco, H. Wang, N.-N. Shen, Y.-J. Gao, X. Zhang, K. Zhu, G.-Y. Zhang and Y.-Y. Liu, *J. Mater. Chem. C*, 2019, **7**, 3049–3055.
5 A. Douvali, A. C. Tsipis, S. V. Eliseeva, S. Petoud, G. S. Papaefstathiou, C. D. Malliakas, I. Papadas, G. S. Armatas, I. Margiolaki, M. G. Kanatzidis, T. Lazarides and M. J. Manos, *Angew. Chem., Int. Ed.*, 2015, **54**, 1651–1656.
6 D. J. Wales, J. Grand, V. P. Ting, R. D. Burke, K. J. Edler, C. R. Bowen, S. Mintova and A. D. Burrows, *Chem. Soc. Rev.*, 2015, **44**, 4290–4321.
7 Z. Z. Ding, G. S. Zheng, Q. Lou, J. F. Han, M. Y. Wu, C. L. Shen, J. H. Zang, K. K. Liu, L. Dong and C. X. Shan, *J. Phys. D: Appl. Phys.*, 2022, **55**, 154001.
8 Y. Wei, Z. Y. Cheng and J. Lin, *Chem. Soc. Rev.*, 2019, **48**, 310–350.
9 L. N. Quan, F. P. García de Arquer, R. P. Sabatini and E. H. Sargent, *Adv. Mater.*, 2018, **30**, 1801996.
10 D.-H. Kwak, D.-H. Lim, H.-S. Ra, P. Ramasamy and J.-S. Lee, *RSC Adv.*, 2016, **6**, 65252–65256.
11 H. Cho, S.-H. Jeong, M.-H. Park, Y.-H. Kim, C. Wolf, C.-L. Lee, J. H. Heo, A. Sadhanala, N. Myoung and S. Yoo, *Science*, 2015, **350**, 1222–1225.

12 L. Hu, G. Shao, T. Jiang, D. Li, X. Lv, H. Wang, X. Liu, H. Song, J. Tang and H. Liu, *ACS Appl. Mater. Interfaces*, 2015, **7**, 25113–25120.
13 K. Ren, L. Huang, S. Yue, S. Lu, K. Liu, M. Azam, Z. Wang, Z. Wei, S. Qu and Z. Wang, *J. Mater. Chem. C*, 2017, **5**, 2504–2508.
14 Z. Zhu, Q. Sun, Z. Zhang, J. Dai, G. Xing, S. Li, X. Huang and W. Huang, *J. Mater. Chem. C*, 2018, **6**, 10121–10137.
15 M. A. Haque, A. Syed, F. H. Akhtar, R. Shevate, S. Singh, K.-V. Peinemann, D. Baran and T. Wu, *ACS Appl. Mater. Interfaces*, 2019, **11**, 29821–29829.
16 Z. Weng, J. Qin, A. A. Umar, J. Wang, X. Zhang, H. Wang, X. Cui, X. Li, L. Zheng and Y. Zhan, *Adv. Funct. Mater.*, 2019, **29**, 1902234.
17 M. Y. Cho, S. Kim, I. S. Kim, E. S. Kim, Z. J. Wang, N. Y. Kim, S. W. Kim and J. M. Oh, *Adv. Funct. Mater.*, 2020, **30**, 1907449.
18 R. Li, J. Yu, S. Wang, Y. Shi, Z. Wang, K. Wang, Z. Ni, X. Yang, Z. Wei and R. Chen, *Nanoscale*, 2020, **12**, 13360–13367.
19 C. Pi, W. Chen, W. Zhou, S. Yan, Z. Liu, C. Wang, Q. Guo, J. Qiu, X. Yu and B. Liu, *J. Mater. Chem. C*, 2021, **9**, 11299–11305.
20 C. Pi, X. Yu, W. Chen, L. Yang, C. Wang, Z. Liu, Y. Wang, J. Qiu, B. Liu and X. Xu, *Mater. Adv.*, 2021, **2**, 1043–1049.
21 Z. Wu, J. Yang, X. Sun, Y. Wu, L. Wang, G. Meng, D. Kuang, X. Guo, W. Qu and B. Du, *Sens. Actuators, B*, 2021, **337**, 129772.
22 W. Xu, F. Li, Z. Cai, Y. Wang, F. Luo and X. Chen, *J. Mater. Chem. C*, 2016, **4**, 9651–9655.
23 X. Zhang, J. Lv, J. Liu, S. Xu, J. Sun, L. Wang, L. Xu, S. Mintova, H. Song and B. Dong, *J. Colloid Interface Sci.*, 2022, **616**, 921–928.
24 Q. A. Akkerman, A. L. Abdelhady and L. Manna, *J. Phys. Chem. Lett.*, 2018, **9**, 2326–2337.
25 L. Wu, H. Hu, Y. Xu, S. Jiang, M. Chen, Q. Zhong, D. Yang, Q. Liu, Y. Zhao, B. Sun, Q. Zhang and Y. Yin, *Nano Lett.*, 2017, **17**, 5799–5804.
26 F. Palazon, C. Urso, L. De Trizio, Q. Akkerman, S. Marras, F. Locardi, I. Nelli, M. Ferretti, M. Prato and L. Manna, *ACS Energy Lett.*, 2017, **2**, 2445–2448.
27 F. Palazon, G. Almeida, Q. A. Akkerman, L. De Trizio, Z. Dang, M. Prato and L. Manna, *Chem. Mater.*, 2017, **29**, 4167–4171.
28 Z. Liu, Y. Bekenstein, X. Ye, S. C. Nguyen, J. Swabeck, D. Zhang, S.-T. Lee, P. Yang, W. Ma and A. P. Alivisatos, *J. Am. Chem. Soc.*, 2017, **139**, 5309–5312.
29 M. Liu, J. Zhao, Z. Luo, Z. Sun, N. Pan, H. Ding and X. Wang, *Chem. Mater.*, 2018, **30**, 5846–5852.
30 X. Y. Yu, L. Z. Wu, H. C. Hu, M. Chen, Y. S. Tan, D. Yang, Q. Pan, Q. X. Zhong, T. Supasai and Q. Zhang, *Langmuir*, 2018, **34**, 10363–10370.
31 Y. X. Li, H. Huang, Y. Xiong, S. V. Kershaw and A. L. Rogach, *CrystEngComm*, 2018, **20**, 4900–4904.
32 X. M. Chen, F. Zhang, Y. Ge, L. F. Shi, S. Huang, J. L. Tang, Z. Lv, L. Zhang, B. S. Zou and H. Z. Zhong, *Adv. Funct. Mater.*, 2018, **28**, 1706567.
33 G. Li, C. She, Y. Zhang, H. Li, S. Liu, F. Yue, C. Jing, Y. Cheng and J. Chu, *Sens. Actuators, B*, 2021, **327**, 128918.
34 H. Huang, M. Hao, Y. Song, S. Dang, X. Liu and Q. Dong, *Small*, 2020, **16**, 1904462.
35 M. Venkatesan, L. Veeramuthu, F.-C. Liang, W.-C. Chen, C.-J. Cho, C.-W. Chen, J.-Y. Chen, Y. Yan, S.-H. Chang and C.-C. Kuo, *Chem. Eng. J.*, 2020, **397**, 125431.
36 D. Xia, J. Li, W. Li, L. Jiang and G. Li, *J. Lumin.*, 2021, **231**, 117784.
37 J. Wei, Y. Ma, C. Liu, J. Li, J. Shen, K. Y. Zhang, S. Liu and Q. Zhao, *J. Mater. Chem. C*, 2021, **9**, 5945–5951.
38 Y. Jiang, Y. Cheng, S. Liu, H. Zhang, X. Zheng, M. Chen, M. Khorloo, H. Xiang, B. Z. Tang and M. Zhu, *Natl. Sci. Rev.*, 2021, **8**, 135.
39 Y. Cheng, J. Wang, Z. Qiu, X. Zheng, N. L. Leung, J. W. Lam and B. Z. Tang, *Adv. Mater.*, 2017, **29**, 1703900.
40 R. Gao, D. Cao, Y. Guan and D. Yan, *Ind. Eng. Chem. Res.*, 2016, **55**, 125–132.
41 T. Liang, W. Liu, X. Liu, Y. Li, W. Wu and J. Fan, *Chem. Mater.*, 2021, **33**, 4948–4959.
42 P. Gao, Z. Cui, X. Liu, Y. Wu, Q. Zhang, Z. Wang, Z. Zheng, H. Cheng, Y. Liu and Q. Li, *Chem. – Eur. J.*, 2022, e202201095.

